Luttinger liquid on a lattice

Zakharov, V.

Chapter 1

Introduction

1.1 Preface

One of the difficult problems in condensed matter physics is treating systems with interactions. An interaction in a Hamiltonian is typically represented by terms that are non-quadratic in quasi-particle creation and annihilation operators. Standard methods based on solving the eigenvalue equation for a single particle then do not apply. The problem becomes intrinsically many-body and must be solved in the full Fock space. The size of the Fock space grows exponentially with the size of the physical system, and quite quickly the problem becomes unsolvable via a direct approach. This obstruction represents the main difficulty in solving many-body physics.

Nevertheless, the development of theoretical physics has produced several ways to deal with the problem of interactions [1]. One of the most well-known theories in this regard is the theory of the Landau liquid [2], whose essential idea is the concept of a quasiparticle. In many materials, the effect of interactions can be efficiently described as a "dressing" of the electron in a cloud of other electrons with which it interacts. The cloud changes the characteristics of the particle, such as its mass or velocity, and gives it a finite lifetime. But ultimately, the quasiparticle can still be described as a free particle.

As famous as the concept of the Fermi liquid is, equally well-known is the fact that it breaks down in one spatial dimension. In 1D, physics can no longer be described with the quasiparticle picture and becomes necessarily strongly correlated. This is why the 1D theory of interacting electrons requires a special name. It is known as the Luttinger or Tomonaga–Luttinger liquid [3, 4]. Despite being truly a many-body problem, the Luttinger liquid is, in the simplest case of

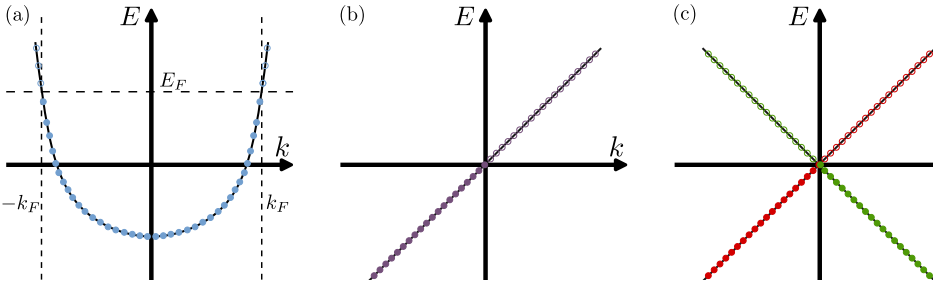

Figure 1.1. Dispersion of one-dimensional electrons for (a) topologically non-protected Luttinger liquid, (b) chiral Luttinger liquid, and (c) helical Luttinger liquid. For (b) and (c) we assume $E_F = 0$ and $k_F = 0$. Filled (empty) circles represent occupied (non-occupied) electron states.

on-site interactions, fully solvable via the bosonization technique. This technique, however, has its limits and cannot solve all variations of the problem — for example, more complicated interactions or the presence of disorder make the problem analytically unsolvable again. Therefore, one would like to have a numerical method capable of describing the physics of such systems.

At the same time, numerical methods for solving Luttinger liquid theory are complicated because of the Nielsen–Ninomiya theorem [5], which prohibits a straightforward discrete formulation of the problem.

These last two facts — the necessity of a numerical method and the simultaneous difficulty of creating one — are the main motivations for the major topic of this thesis. In the remainder of the introduction, I will formally define the Luttinger liquid and describe its main characteristics, as well as introduce the concept of the bosonization technique and briefly describe the lattice formulation of the problem and the no-go theorem.

1.2 Topologically protected Luttinger liquid

The standard image of a Luttinger liquid dispersion, i.e., the non-interacting part of the energy, is presented in Figure 1.1. Panel (a) represents a generic band with finite filling, far from the ends of the band. In one spatial dimension, such a band has two points where the Fermi energy E_F crosses the dispersion. In the vicinity of these crossings, one may approximate the dispersion as

$$E(k) \approx \pm v_F(\hat{k} \pm k_F) + E_F. \tag{1.1}$$

Calling the corresponding eigen-wavefunctions Ψ_R and Ψ_L, and making a matching transformation $\hat{k} \to \hat{k} \mp k_F$, one defines an effective one-dimensional problem of an electron with a quasi-spin:

$$H\Psi = E\Psi, \quad H = v_F \sigma_z \hat{k}. \tag{1.2}$$

This Hamiltonian describes a gapless (metallic) system in one dimension. But the gaplessness in this picture is not protected and results from fine-tuning. Since both Ψ_R and Ψ_L come from the same electronic band, nothing prevents a generic term in the initial Hamiltonian that would couple the k_F and $-k_F$ points — for instance, a random disorder. Coupling of these two points is a backscattering process that introduces an effective mass term $m\sigma_x$ to the Hamiltonian (1.2) and opens a gap in the spectrum.

To protect the metallic behavior, one needs to rely on topological protection. In other words, the quasi-spin of the electron must be a symmetry-protected quantum number. One such system is a chiral fermion with a dispersion shown in Figure 1.1 (b). In one dimension chiral fermion is defined by its velocity direction, it is strictly a right- or left-mover. The absence of a counter-propagating electron makes backscattering impossible and therefore topologically guarantees gaplessness. A one-dimensional interacting system with a single chiral electron mode is then called a chiral Luttinger liquid, whose Hamiltonian in the non-interacting limit is simply

$$H = v_F \hat{k}. \tag{1.3}$$

Obviously, adding any number of additional fermions with the same chirality cannot open a gap either, since backscattering remains impossible. A physical example of such a system in condensed matter is the edge of a quantum Hall system [6], schematically represented in Figure 1.2 (a), which is topologically equivalent to a one-dimensional ring with all electrons being chiral right- or left-movers.

Moreover, one may also include pairs of different fermions with opposite chiralities without spoiling the metallic behavior, as long as their chirality is protected. The minimal example of one right- and one left-mover is shown in Figure 1.1 (c) and described by the same Hamiltonian as in (1.2), but now with chirality as a well-defined quantum number fixed by the band. The absence of a backscattering process is typically guaranteed by time-reversal (TR) symmetry: the Hamiltonian must be invariant under the transformation $(\sigma, \hat{k}) \to (-\sigma, -\hat{k})$. This model is called a helical Luttinger liquid and is physically realized at the edge of a quantum spin Hall insulator [7, 8], illustrated in Figure 1.2 (b).

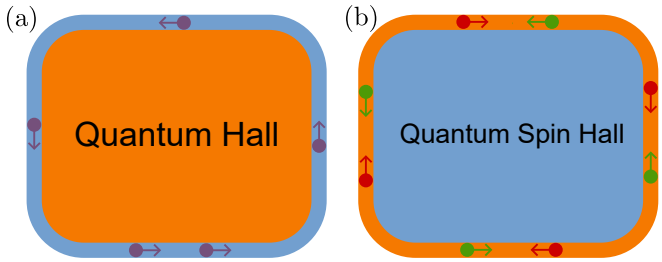

Figure 1.2. Schematic representation of (a) a Quantum Hall insulator and (b) a Quantum Spin Hall insulator. Both systems are insulating in the bulk and have conducting edges. Propagating electrons, represented by dots at the boundaries, are chiral; their velocity, illustrated by small arrow-vectors, is determined either by (a) the topology of the system or by (b) their (quasi-)spin depicted by different colors. The edges are quasi-one-dimensional, conducting, and topologically protected, and therefore represent a physical realization of a Luttinger liquid system.

Platforms that experimentally realize the physics of chiral or helical Luttinger liquids include the topological states of matter mentioned above, as well as composite systems such as Josephson junction chains and cold atoms [9].

1.3 Chiral fermions in QFT and SPT

Although the title of this thesis is "Luttinger liquid on a lattice," and most chapters focus on the specific example of a helical Luttinger liquid, the key ingredient in that physical picture is the concept of a one-dimensional chiral fermion, as discussed in Section 1.2. This concept plays a crucial role both in quantum field theories in (1+1)D and in symmetry-protected topological (SPT) phases of matter in 2D. Accordingly, the numerical methods developed in this thesis are also highly relevant to these broader areas. In this section, I briefly describe how the concept of chiral fermions arises in QFT and SPT phases.

Fermions in quantum field theory are spinors described by the Dirac equation,

$$S = \int \mathrm{d}^2x\overline{\psi}\left(i\gamma^0\partial_t + i\gamma^1\partial_x + m\right)\psi, \tag{1.4}$$

where $\overline{\psi} = \psi^\dagger\gamma^0$, and the gamma matrices $\gamma^0 = \sigma_x$, $\gamma^1 = i\sigma_y$ satisfy the Clifford algebra $\{\gamma^\mu, \gamma^\nu\} = 2\eta^{\mu\nu}$ with $\eta^{\mu\nu} = \mathrm{diag}(1, -1)$. When the fermion is massless ($m = 0$), the action simplifies to

$$S = \int \mathrm{d}^2x i\psi^\dagger\left(\partial_t - \gamma^5\partial_x\right)\psi, \tag{1.5}$$

where $\gamma^5 = -\gamma^0\gamma^1 = \sigma_z$. In this form, the massless Dirac fermion decouples into two independent chiral components $\psi_\pm = \frac{1}{2}(1 \pm \gamma^5)\psi$. Thus, the original vector ($\psi \to e^{i\alpha}\psi$) and axial ($\psi \to e^{i\alpha\gamma^5}\psi$) symmetries of the theory become two independent chiral symmetries: $\psi_\pm \to e^{i\alpha_\pm}\psi_\pm$.

An SPT phase of matter [10] is a type of topological insulator (TI), characterized by a gapped bulk and a gapless, symmetry-protected edge. In this sense, a quasi-1D edge of a 2D TI provides a natural platform to realize Luttinger liquid physics. TIs can exhibit either short-range or long-range entanglement. Here, we focus on short-range entangled TIs, known as SPT phases, which, in contrast to long-range entangled TIs, do not support intrinsic topological order such as fractional statistics (as seen, for instance, in the fractional quantum Hall effect).

SPT phases generalize the notion of topological band insulators (TBIs) to include interactions. Hence, examples like the integer quantum Hall state and the quantum spin Hall state discussed in the previous section are both fermionic SPT phases in two dimensions. Further, fermionic SPT phases include many-body interacting states that cannot be realized within a free-particle picture [11]. The boundaries of these more exotic phases can often be described by multicomponent Luttinger liquid theories [12].

1.4 Bosonization

The fundamental features of Luttinger liquid physics can be captured analytically using the method of bosonization [13]. Here we consider a helical system on a ring of length L, with the dispersion shown in Fig. 1.1(c), described by the Hamiltonian

$$H = \int_{-L/2}^{L/2} \mathrm{d}x :\left[\psi_\uparrow^\dagger(-iv_F\partial_x)\psi_\uparrow - \psi_\downarrow^\dagger(-iv_F\partial_x)\psi_\downarrow + g_1\hat{\rho}_\uparrow(x)\hat{\rho}_\downarrow(x) + g_2\left(\hat{\rho}_\uparrow^2(x) + \hat{\rho}_\downarrow^2(x)\right)\right]:, \tag{1.6}$$

where $\psi_\sigma = \frac{1}{\sqrt{L}}\sum_k e^{-ikx}c_{k,\sigma}$ and $\rho_\sigma = \psi_\sigma^\dagger\psi_\sigma$. The terms with coefficients g_1 and g_2 represent density-density interactions between opposite and same chirality, respectively. Colons denote normal ordering. In this regime, the model becomes analytically solvable in the bosonic representation [14]. In this section I briefly describe how to do it.

We construct bosonic operators as bilinears of fermionic operators:

$$b_{q\sigma} = -\frac{i}{\sqrt{n_q}} \sum_k c^\dagger_{k-q,\sigma} c_{k,\sigma}, \quad q = \frac{2\pi}{L}\sigma n_q, \quad n_q > 0,$$
$$\phi_\sigma(x) = -\sum_{n_q} \frac{1}{\sqrt{n_q}} \left[e^{-iqx} b_{q\sigma} e^{-a\sigma q/2} + e^{iqx} b^\dagger_{q\sigma} e^{-a\sigma q/2} \right]. \tag{1.7}$$

where $b_{q\sigma}$ is a bosonic annihilation operator and $\phi_\sigma(x)$ is the bosonic field. The ultraviolet regularization parameter a is introduced to control divergences of the theory.

Now the fermionic fields and densities can now be expressed in terms of $\phi_\sigma(x)$ via the famous bosonization transformation:

$$\rho_\sigma(x) = \frac{1}{L}\hat{N}_\sigma + \frac{\sigma}{2\pi}\partial_x \phi_\sigma(x), \tag{1.8}$$
$$\psi(x)_\sigma = \frac{1}{\sqrt{2\pi a}} F_\sigma e^{-i\sigma\frac{2\pi}{L}(\hat{N}_\sigma - [1-\delta_b]/2)x} e^{-i\phi_\sigma(x)}. \tag{1.9}$$

Here, since by the construction the bosonic operators can not measure the total amount of fermions in the system, we introduced $\hat{N}_\sigma$ as the total number of electrons counted from the half-filling point. Correspondingly we define the $|N_\sigma\rangle$ states as the ground states of the non-interacting Hamiltonian with fixed amount of electrons. In other words $\left|N_\uparrow\right\rangle$ is a state with all $\left|(k < -\frac{2\pi n}{L}, \sigma = \uparrow)\right\rangle$ filled and respectively $\left|N_\downarrow\right\rangle$ is a state with all $\left|(k > \frac{2\pi n}{L}, \sigma = \downarrow)\right\rangle$ filled. Obviously the eigenvalue relation $\hat{N}_\sigma |N_\sigma\rangle = N_\sigma$ holds. Additionally, to be able to switch between different $|N_\sigma\rangle$ states, and to satisfy the fermionic statistic the Klein factors F_σ are being introduced as

$$F_\sigma |N_\sigma\rangle = T_\sigma |N_\sigma - 1\rangle, \quad T_\downarrow = (-1)^{N_\uparrow}, \quad T_\uparrow = 1. \tag{1.10}$$

Substituting the bosonization relation (1.8) into Eq. (1.6), the Hamiltonian becomes [14]

$$H = \frac{\pi v}{L}\Bigg[\sum_\sigma (\frac{1}{g} + g) \left(\frac{1}{2}\hat{N}^2_\sigma + \sum_{n_q} n_q b^\dagger_{q\sigma} b_{q\sigma} \right)$$
$$+ (\frac{1}{g} - g) \left(\hat{N}_\uparrow \hat{N}_\downarrow - \sum_{n_q} n_q \left[b^\dagger_{q\uparrow} b^\dagger_{q\downarrow} + b_{q\uparrow} b_{q\downarrow} \right] \right) \Bigg] + \delta_b \sum_\sigma \frac{\pi v_F}{L} N_\sigma, \tag{1.11}$$

where the renormalized velocity v and dimensionless electron-electron interaction parameter g ($g = 1$ for the free case) are given by

$$v = v_F \sqrt{\left(1 + \frac{g_2}{\pi v_F}\right)^2 - \frac{g_1^2}{4\pi^2 v_F^2}}, \quad g = \sqrt{\frac{v_F + g_2/\pi - g_1/(2\pi)}{v_F + g_2/\pi + g_1/(2\pi)}}. \tag{1.12}$$

In Eq.(1.11) the term with coefficient $(\frac{1}{g} + g)$ corresponds to the kinematic part of the initial Hamiltonian, the $(\frac{1}{g} - g)$ term comes from the interacting part, and the last term originates from the finite size formulation with $\delta_b = 1$ for periodic boundary conditions and $\delta_b = 0$ if it is antiperiodic.

Finally, the beauty of the bosonization idea becomes visible: the interaction terms, originally quartic in the fermionic formulation, become quadratic in the bosonic representation. This bosonic Hamiltonian can be diagonalized via a Bogoliubov transformation:

$$B_{q\pm} = \frac{1}{\sqrt{8}} \left[\left(\frac{1}{\sqrt{g}} + \sqrt{g} \right) \left(b_{q\uparrow} \mp b_{q\downarrow} \right) \pm \left(\frac{1}{\sqrt{g}} - \sqrt{g} \right) \left(b^\dagger_{q\uparrow} \mp b^\dagger_{q\downarrow} \right) \right],$$
$$H = \frac{2\pi v}{L} \sum_\sigma \sum_{n_q} n_q B^\dagger_{q\sigma} B_{q\sigma} + \sum_\sigma \frac{\pi v_F}{L} N_\sigma \left[N_\sigma + \delta_b \right] + \frac{g_1}{L} N_\uparrow N_\downarrow + \sum_\sigma \frac{g_2}{L} N_\sigma^2. \tag{1.13}$$

Thus, the Luttinger liquid model defined in Eq. (1.6) is solved analytically. With access to the full eigenspectrum and eigenfunctions, one can compute various observables such as Green's functions or spin correlators, which exhibit power-law behavior characteristic of gapless one-dimensional systems. In Chapter 2, we calculate these correlators, carefully taking finite-size and finite-temperature effects into account, to compare the analytical predictions with our numerical simulations.

1.5 Lattice formulation and no-go theorem

In the previous sections, we described the fundamentals of the helical Luttinger liquid and showed that, in its simplest form, it is fully analytically solvable. Bosonization is a powerful tool that provides deep insights into the physics of chiral fermions in one dimension. Nevertheless, not all scenarios can be solved analytically. Breaking translational symmetry, via disorder or scalar potentials, or introducing more complex interactions, such as spatially dependent terms or higher-order fermionic operators, makes the model analytically intractable.

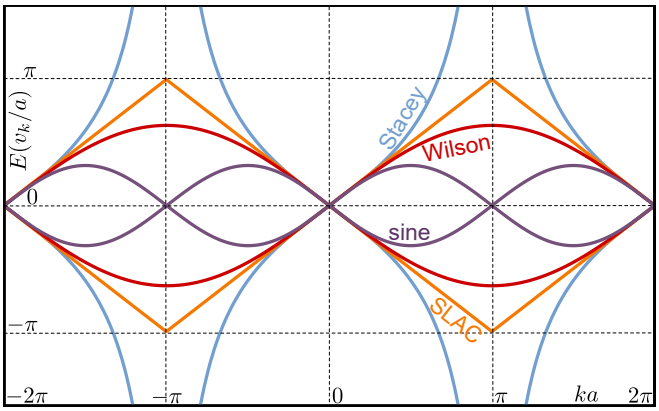

Figure 1.3. Dispersion relations of free electrons resulting from different discretization schemes of the Dirac Hamiltonian in one dimension, shown over two Brillouin zones. Only the Stacey derivative simultaneously preserves chiral symmetry, avoids doublers, and supports efficient numerical simulations due to hidden locality.

Therefore, one would like to simulate Luttinger liquid physics *in silico*, ideally in a numerically efficient manner. Or, in other words, to put the *Luttinger liquid on a lattice*. However, one immediately encounters the nontrivial problem of discretizing the momentum operator:

$$\hat{k} = -i\partial_x. \tag{1.14}$$

This obstacle is known as the fermion-doubling problem, formalized in the no-go theorem by Nielsen and Ninomiya [5]:

Any hermitian and local in real space Hamiltonian
that preserves the chirality of the Dirac fermions
must have an even number of left- and right-movers in the Brillouin zone.

Here we illustrate this phenomenon (see also Fig. 1.3) with several examples that implement different discretization schemes of the Dirac Hamiltonian:

$$H_D = -iv_F\sigma_z\partial_x = v_F\sigma_z\hat{k}. \tag{1.15}$$

Sine derivative

The most straightforward discretization of the derivative is the central finite difference:

$$\partial_x f(x) \to (2a)^{-1}(f(x+a) - f(x-a)). \tag{1.16}$$

In momentum space, this leads to a sine dispersion:

$$H_D \to H_{sin} = v_F/a\sigma_z \sin(\hat{k}a). \tag{1.17}$$

This formulation is local and chiral symmetric ($H_{\sin} \propto \sigma_z$), but, consistent with the no-go theorem, it results in a doubler with opposite chirality at the Brillouin zone (BZ) edge (see Figure 1.3). As discussed in Section 1.2, the presence of doublers results in the theory unstable to disorder or generic inter-cone coupling, making it incapable for simulating Luttinger liquid physics.

Wilson derivative

To resolve the doubling problem in Eq. (1.17), one can add a momentum-dependent mass term to gap out the unwanted cone:

$$H_D \to H_{Wilson} = v_F/a \left[\sigma_z \sin(\hat{k}a) + \left(1 - \cos(\hat{k}a)\right)\sigma_x\right]. \tag{1.18}$$

This formulation of discretized Dirac Hamiltonian has a name of Wilson fermion. Certainly it is still local ($\cos(\hat{k}a)$ is a sparce matrix in real space) and eliminates the doubler. However, it explicitly breaks chirality by introducing a σ_x mass term that mixes the chiralities, violating a key assumption of the Nielsen-Ninomiya theorem. This term needs to be fine-tuned in order to vanish at $k = 0$ and therefore it is unstable to disorder. Furthermore, it reintroduces chirality mixing away from $k = 0$ (see how at Figure 1.3 dispersions of left- and right-mover of Wilson discretization smoothly merge at the edge of the BZ), resulting in backscattering and undermining the chiral nature of the system.

SLAC derivative

From the previous schemes, we see that either explicit chirality breaking (Wilson) or the presence of doublers (sine) obstructs the topological protection of the chiral fermion on a lattice. Therefore the only remaining assumption of the no-go theorem that can be relaxed is the locality of the derivative operator in real space. One of the formulation exploiting this idea is called SLAC derivative

$$\partial_x f(x) \to \sum_{n=1}^{\infty} (-1)^n (an)^{-1} (f(x+na) - f(x-na)). \tag{1.19}$$

As depicted at the Figure 1.3 it produces a Hamiltonian that is strictly linear in momentum

$$H_D \to H_{SLAC} = v_F/(ia)\sigma_z \ln e^{i\hat{k}a}. \tag{1.20}$$

Ultimately, SLAC lattice formulation produces a strictly chiral fermion without a doubler by the cost of being non-local, making it a reasonable candidate for simulating chiral physics. However, attempts of reproducing the Luttinger liquid behavior within SLAC framework seem to fail [15] presumably due to the utter non-locality of SLAC fermion.

Stacey derivative

An alternative non-local discretization is provided by the Stacey derivative [16]:

$$\partial_x f(x) \to 2(a)^{-1} \sum_{n=1}^{\infty} (-1)^n (f(x+na) - f(x-na)). \tag{1.21}$$

This leads to the tangent dispersion (see Figure 1.3) in momentum space:

$$H_D \to H_{tan} = 2v_F/a\sigma_z \tan\left(\hat{k}a/2\right). \tag{1.22}$$

This discretization scheme, called the *tangent fermion* [17], plays a central role in this thesis and lays in the foundation of the numerical methods developed herein.

Tangent fermion is highly non-local in its' original formulation. Namely, Eq. (1.21) contains all-to-all hoppings of the same, not-decaying amplitude. Remarkably, tangent fermion, as it explained in the Chapter 3, possess hidden locality, which allows for various efficient local formulations. Furthermore, it accomplishes the task of reproducing Luttinger liquid physics faithfully, a success we attribute to its' unique combination of chirality preservation and hidden locality.

1.5.1 Domain wall fermion

Finally it is worth to mention here another approach to circumvent the fermion doubling. It has the name of domain wall fermion and exploits the idea of reproducing the physics of one-dimensional chiral fermions as the edge state of a two-dimensional topological system, thereby lifting the dimensionality of the system from 1D to 2D. While being rigorous, this formulation is consequentially more demanding numerically since one needs to simulate a system of a greater dimensionality. Further, it introduces an unavoidable bulk-edge coupling, which compromises the intrinsic one-dimensional character of the model.

1.6 This thesis

During my PhD journey I encountered and worked on several different topics in theory of condensed matter. The physics of strongly correlated chiral fermions in one dimension became the main focus of my PhD, two chapters of this thesis represent it. In Chapter 2 we implement the idea of tangent fermions to simulate the helical Luttinger liquid using quantum Monte Carlo (QMC) approach, and then we extend the idea further to tensor network methods in Chapter 3. The remaining two chapters of this thesis focus on two-dimensional single-particle physics. In Chapter 4 we study the Majorana metal transition as a percolation of topological edge modes. Finally, Chapter 5 investigates the phenomenon of Landau quantization in systems with generalized Van Hove singularities. Below, I summarize the main results of each chapter.

1.6.1 Chapter 2

In this chapter we tackle the significant challenge in simulating strongly correlated one-dimensional systems for the first time. We choose helical Luttinger liquid as a test ground, an ideal candidate to do the benchmark of our method due to its analytical solvability. We introduce a novel approach using tangent fermions on a space-time lattice. This method possess the hidden locality that makes numerical simulations feasible, while preserving the chirality of the fermions and removing the doublers. Namely the approach has a local Euclidean action formulation which is applicable in Quantum Monte Carlo (QMC) simulations.

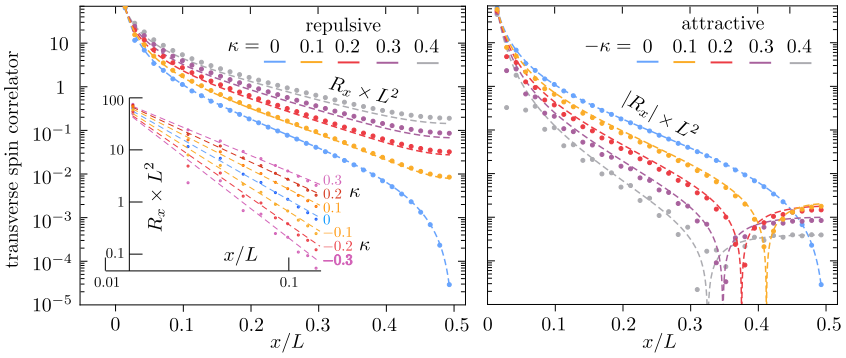

Figure 1.4. Quantum Monte Carlo results (data points) for the spin correlator of a helical Luttinger liquid on a space-time lattice, showing excellent agreement with analytical bosonization theory (dashed curves) for both repulsive and attractive interactions. This validates the tangent fermion approach for simulating correlated systems.

Crucially, our fermionic auxiliary-field QMC simulations for the helical Luttinger liquid at half-filling are shown to be sign-problem-free, a common challenge in fermionic simulations. The results from our simulations accurately reproduce the expected Luttinger liquid continuum physics without needing any adjustable parameters. We validate our findings by comparing them with analytical bosonization theory, even deriving finite-size and finite-temperature corrections for precise comparisons. This work represents a significant step as the first successful lattice simulation of the helical Luttinger liquid.

1.6.2 Chapter 3

Following the successful validation of the tangent fermion approach using QMC in Chapter 2, this chapter pushes the boundaries further by employing powerful tensor network methods, specifically the Density Matrix Renormalization Group (DMRG). While QMC proved the concept, it was limited by the sign problem to specific conditions like helical systems at half-filling without external potentials. Tensor networks offer a way to overcome these limitations.

We demonstrate that the hidden locality inherent in the tangent fermion formulation allows for an efficient representation using tensor networks. This finding, coupled with the non-locality required by the Nielsen-Ninomiya theorem to avoid fermion doubling and the necessity of preserving well-defined chirality, provides strong support for the uniqueness of the tangent fermion approach.

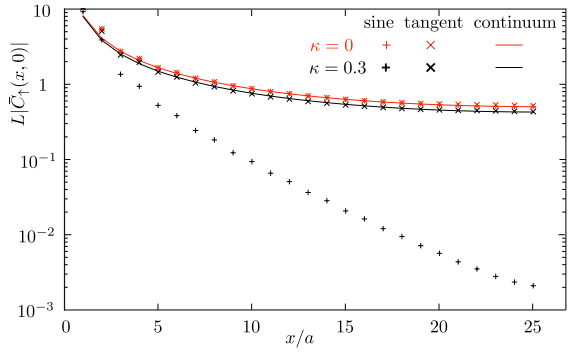

Figure 1.5. Absolute value of the propagator calculated using tensor networks for the tangent (dots) and sine (plusses) discretizations of the Luttinger Hamiltonian. The tangent discretization agrees well with the continuum analytical results (curves), while the sine discretization shows an unphysical gap. This highlights the advantage of the tangent fermion approach.

Using DMRG, we achieve excellent agreement between our results and

bosonization theory. We also perform a critical comparison with a straightforward sine discretization formulation, which, in contrast, results in a gapped spectrum, highlighting the instability of lattice formulations burdened by fermion doublers. This work establishes tensor networks as a viable and versatile tool for simulating strongly correlated chiral fermions on a lattice using the tangent fermion framework.

1.6.3 Chapter 4

This chapter delves into the behavior of disordered chiral p-wave superconductors, a type of topological material classified by the Chern number. While conventional superconductors are typically thermal insulators, disorder can transform these topological superconductors into a thermal metal phase, where heat is transported by Majorana fermions. The transition to this Majorana metal phase has been observed in computer simulations but not yet experimentally.

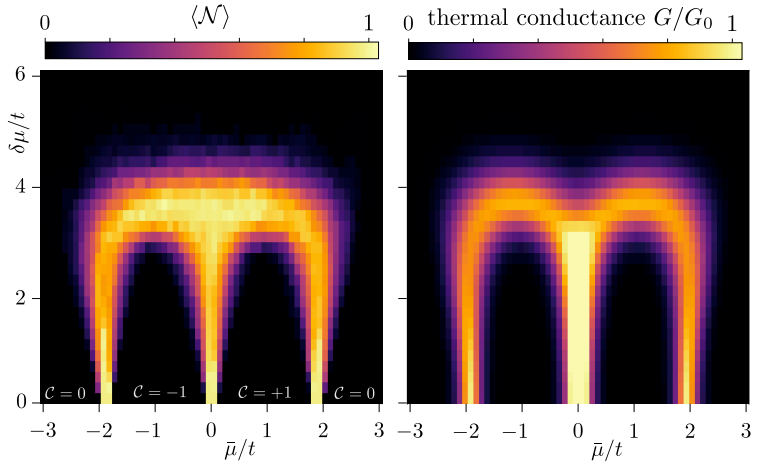

Figure 1.6. Left panel shows the average number of percolating domain walls as a function of disorder parameters, clearly distinguishing the region where the Majorana metal phase emerges. Right panel shows the corresponding thermal conductance, confirming the transition. This demonstrates that the thermal metal-insulator transition is driven by the percolation of topological domain walls.

Our research provides compelling numerical evidence that this thermal metal – insulator transition occurs via the percolation of boundaries separating regions with different topological properties (specifically, different Chern numbers). In a clean system, the Chern number is uniform, making the bulk insulating. How-

ever, disorder creates a "topological landscape" of domains with varying Chern numbers.

To study this process in real space, we employ the innovative concept of the spectral localizer, which acts as a "topological landscape function" capable of determining local Chern numbers. This allows us to visualize the formation of a network of domain walls between these topologically distinct domains. As disorder increases, these domains grow and eventually connect, forming a percolating cluster that spans the system, providing a channel for Majorana fermions and enabling thermal conduction. By analyzing this percolation transition, we successfully determine the thermal metal–insulator phase diagram.

1.6.4 Chapter 5

This chapter explores the phenomenon of magnetic breakdown in 2D materials, particularly focusing on regions with generalized Van Hove singularities (vHs). Magnetic breakdown occurs when electron trajectories in a magnetic field come close together, allowing quantum tunneling. While well-studied at usual vHs, newer 2D materials feature "high-order" vHs with flatter dispersions, leading to richer magnetic breakdown behavior and new challenges.

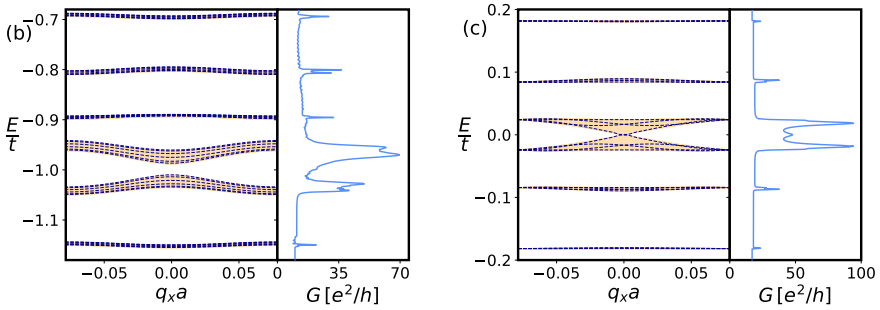

Figure 1.7. Longitudinal conductance (right panels, blue lines) calculated for finite systems with (b) square lattice and A_3 saddle point and (c) triangular lattice and Monkey saddle point, compared with the spectral structure of Landau minibands (left panels, orange solid lines (tight-binding simulations) and blue dashed lines (analytically via our approach)) arising from coherent orbit networks connected via magnetic breakdown at different types of Van Hove singularities. The conductance peaks correspond to the minibands, demonstrating the possibility of bulk conduction mediated by these networks.

We develop a general method to calculate the precise magnetic breakdown scattering matrix (s-matrix) for any type of saddle point, including these high-

order cases. Our approach maps the problem onto a 1D scattering problem in a quantum chain derived from the Landau level basis.

A key consequence of magnetic breakdown, especially when saddle points are at the edge of the Brillouin zone, is the formation of coherent orbit networks. These networks delocalize the Landau level states, forming dispersive Landau mini-bands that can support bulk electrical conduction in the presence of a magnetic field. We calculate the longitudinal bulk conductance in a quantum Hall bar geometry and show that this conduction, enabled by the orbit networks, can strongly exceed the standard edge conductance. The energy-dependent width of these mini-bands (and thus the conductance peaks) is uniquely tied to the type of vHs, offering a potential experimental signature to distinguish between different types of saddle points through conductance measurements.